International Journal of Microscale and Nanoscale Thermal … ISSN: 1949-4955
Volume 4, Number 2

NON-DARCY NATURAL CONVECTION OF A NANOFLUID ABOUT A PERMEABLE VERTICAL CONE EMBEDDED IN A POROUS MEDIUM

Ali J. Chamkha[1], A. M. Rashad[2], and Abdelraheem M. Aly[3, 4]
[1]Manufacturing Engineering Department,
The Public Authority for Applied Education and Training, Shuweikh, Kuwait
[2]Department of Mathematics, Aswan University, Faculty of Science, Aswan, Egypt
[3]Department of Mathematics, South Valley University, Faculty of Science, Qena, Egypt
[4]Civil Engineering Department, Faculty of Engineering, Kyushu University, Japan

ABSTRACT

An analysis is performed to study the effect of uniform wall transpiration on non-Darcy free convection boundary-layer flow over a permeable vertical cone embedded in a porous medium saturated with a nanofluid. The model used for the nanofluid incorporates the effects of Brownian motion and thermophoresis.

The governing partial differential equations are transformed into a set of non-similar equations and solved numerically by an efficient implicit, iterative, finite-difference method. Comparisons with previously published work are performed and excellent agreement is obtained.

Numerical results are obtained for the velocity, temperature and nanoparticles volume fraction profiles, as well as the friction factor, local Nusselt number and the local Sherwood number for several values of the parameters, namely, the Ergun number Er ranging from 0.0 to 0.6, Lewis number Le ranging from 1.0 to 20, buoyancy ratio parameter Nr ranging from 0.1 to 0.7, Brownian motion parameter *Nb* ranging from 0.1 to 0.7, thermophoresis parameter *Nt* ranging from 0.1 to 0.7 and the transpiration parameter ξ ranging from 0.1 to 0.7.

The obtained results are presented graphically and in tabular form and the physical aspects of the problem are discussed.

It is found that an increase in either of the Ergun number, buoyancy ratio parameter, thermophoresis parameter or the transpiration parameter leads to a decrease in the local Nusselt number and the local Sherwood number whereas the opposite behavior occurs with increasing the Lewis number. In addition, increasing of the Brownian motion parameter causes a decrease in the local Nusselt number and an increase in the local Sherwood number.

Keywords: Natural convection; non-Darcy; porous medium; nanofluid; thermophoresis

NOMENCLATURE

C nanoparticle volume fraction [nm]
C_w nanoparticle volume fraction at the vertical plate [nm]
C_∞ ambient nanoparticle volume fraction attained as y tends to infinity [nm]
d the pore diameter [m]
D_B Brownian diffusion coefficient [m^{-2} s^{-1}]
D_T thermophoretic diffusion coefficient [m^{-2} s^{-1}]
Er Ergun number (non-Darcy number) (equation 7)
f dimensionless stream function
g gravitational acceleration vector [m s^{-2}]
K permeability of porous medium [m^2]
K^* porous medium inertial coefficient [m^{-1}]
k_f thermal conductivity [w $m^{-1}K^{-1}$]
Le Lewis number (equation 9)
Nr Buoyancy Ratio (equation 7)
Nb Brownian motion parameter (equation 8,9)
Nt thermophoresis parameter (equation 8,9)
Nu_x local Nusselt number
r radius of the cone [m]
Ra_x Modified local Rayleigh number
Sh_x local Sherwood number
T temperature [K]
T_W temperature at vertical plate [K]
T_∞ ambient temperature attained as y tends to infinity [K]
V_w wall suction or injection velocity [ms^{-1}]
u,v velocity components [ms^{-1}]
(x,y) Cartesian coordinates [m]

Greek Symbols

α thermal diffusivity of porous medium [m^2 s^{-1}]
β volumetric expansion coefficient of fluid [K^{-1}]
γ half angle of the cone [^{o}]
μ dynamic viscosity [N s m^{-2}]
η similarity parameter
θ dimensionless temperature
ϕ dimensionless nano-particle volume fraction
ψ stream function (m^3 s^{-1})
ρ_f fluid density (Kg m^{-3})
ρ_p nano-particle mass density (Kg m^{-3})
$(\rho c)_f$ heat capacity of the fluid (J Kg^{-1} K^{-1})
$(\rho c)_p$ effective heat capacity of nano-particle material (J Kg^{-1} K^{-1})
τ parameter defined by equation
ξ the transpiration parameter

Subscripts

w conditions at the wall
∞ conditions in the free stream

1. INTRODUCTION

Convective heat transfer from surfaces embedded in porous media has been the topic of several studies in recent year. This interest in the subject stems from various engineering applications in geothermal reservoirs, petroleum industries, transpiration cooling, storage of nuclear waste materials, separation processes in chemical industries, building thermal insulation, and solar heating systems. Early work on porous media used the Darcy law that neglects important effects such as boundary and inertia effects. Vafai and Tien [1] have reported a pioneering work on the boundary and inertia effects of porous media on convective flow and heat transfer situations. In recent years, enhanced models of porous media have been reported. These models have been applied for simulating more generalized situations such as flow through packed and fluidized beds and liquid metal flow through dendritic structures in alloy casting (Nithiarasu et al. [2]). Some of these models deal with variable porosity effects near the boundary in which the porosity distribution exhibits a peak value there and then decays asymptotically beyond that value. The basis for these models was the early experimental work of Benenati and Brosilow [3] on void fraction distribution in packed beds. Examples of such models are reported and employed by Vafai [4], Vafai et al. [5], Poulikakos and Renken [6] and Nithiarasu et al. [2]. Other models have dealt with thermal dispersion or secondary flow effects in porous media which result from mixing and recalculation of local fluid particles through tortuous paths formed by the spherical particles in packed beds. Examples of these models have been reported by Cheng and Vortmeyer [7] and Amiri and Vafai [8]. Also, Darcy's law has been the momentum equation used in many studies of fluid flow in porous media. Because Darcy's law is of order one less than the Navier–Stokes equation, only the impermeable boundary condition at a surface can be satisfied; the no-slip boundary condition cannot. In contrast with rocks, soil, sand, and other media that do fall within this category, certain porous materials, such as foam metals and fibrous media, usually have high porosities. In these media, the boundary and inertia effects not included in Darcy's model may alter the flow and heat transfer characteristics. It is therefore, necessary to determine the conditions under which these effects are important. When the Reynolds number based on the pore size is greater than unity and there is an impermeable boundary or wall, the non-Darcy effects (the inertia and boundary effects) should be included in the momentum equation. The inertia effects can be accommodated through the so-called Forchheimer's extension, while the boundary effects can be modeled, in a formalization known as Brinkman's extension, through the inclusion of a viscous shear stress term.

Nanofluids are prepared by dispersing solid nanoparticles in fluids such as water, oil, or ethylene glycol. These fluids represent an innovative way to increase thermal conductivity and, therefore, heat transfer. Unlike heat transfer in conventional fluids, the exceptionally high thermal conductivity of nanofluids provides for exceptional heat transfer, a unique feature of nanofluids. Advances in device miniaturization have necessitated heat transfer systems that are small in size, light mass, and high-performance. Several authors have tried to

establish convective transport models for nanofluids. Xuan et al. [9] have examined the transport properties of nanofluid and have expressed that thermal dispersion, which takes place due to the random movement of particles, takes a major role in increasing the heat transfer rate between the fluid and the wall. This requires a thermal dispersion coefficient, which is still unknown. Brownian motion of the particles, ballistic phonon transport through the particles and nanoparticle clustering can also be the possible reason for this enhancement [10]. Das et al. [11] has observed that the thermal conductivity for a nanofluid increases with increasing temperature. They have also observed the stability of Al_2O_3–water and CuO–water nanofluid. Experiments on heat transfer due to natural convection with nanofluid have been studied by Putra et al. [12] and Wen and Ding [13]. They have observed that heat transfer decreases with increase in concentration of nanoparticles. The viscosity of this nanofluid increases rapidly with the inclusion of nanoparticles as the shear rate decreases. Chamkha et al. [14] have studied mixed convection MHD flow of a nanofluid past a stretching permeable surface in the presence of magnetic field, heat generation or absorption, thermopherosis, Brownian motion and suction or injection effects. Chamkha et al. [15] have also analyzed natural convection past a sphere embedded in a porous medium saturated by a nanofluid. Gorla et al. [16] have studied steady boundary layer flow of a nanofluid on a stretching circular cylinder in a stagnant free stream. Gorla et al. [17] have analyzed mixed convection past a vertical wedge embedded in a porous medium saturated by a nanofluid.

In this study, the effect of uniform wall transpiration on non-Darcy free convection boundary-layer flow over a permeable vertical cone embedded in a porous medium saturated with a nanofluid is considered. The model used for the nanofluid incorporates the effects of Brownian motion and thermophoresis. Numerical solutions of the boundary layer equations are obtained and discussion is provided for several values of the nanofluid parameters governing the problem. The dependency of velocity, temperature and nanoparticles volume fraction profiles as well as the local Nusselt number and local Sherwood number on these parameters are discussed.

2. GOVERNING EQUATIONS

Consider the problem of free convection boundary-layer flow of a Newtonian nanofluid over a permeable vertical cone embedded in a porous medium in the presence of uniform wall transpiration effects. The model used for the nanofluid incorporates the effects of Brownian motion and thermophoresis. It assumed that the cone surface is maintained at a constant temperature T_w and a constant nanoparticles volume fraction C_w and the ambient temperature and nanoparticles volume fraction far away from the surface of the cone T_∞ and C_∞ are assumed to be uniform. For $T_w>T_\infty$ and $C_w>C_\infty$ an upward flow is induced as a result of the thermal and nanoparticle volume fraction buoyancy effects.

Figure 1 shows the flow model and the physical coordinate system. The origin of the coordinate system is placed at the vertex of the cone, where x and y are the Cartesian coordinates measuring the distances along and normal to the surface of cone, respectively. For the flow in the porous medium, the non-Darcy model proposed by Ergun [18] is adopted in this work. The governing equations for the problem under consideration with the boundary layer and Boussinesq approximations and the modified non-Darcy law can be written as (see Yih [19]):

$$\frac{\partial(ru)}{\partial x}+\frac{\partial(rv)}{\partial y}=0, \tag{1}$$

$$\frac{\partial u}{\partial y}+\frac{\rho_{f\infty}K^{*}}{\mu}\frac{\partial u^{2}}{\partial y}=\frac{(1-C_{\infty})\rho_{f\infty}\cos\gamma\beta gK}{\mu}\frac{\partial T}{\partial y}-\frac{(\rho_{p}-\rho_{f\infty})\cos\gamma gK}{\mu}\frac{\partial C}{\partial y}, \tag{2}$$

$$u\frac{\partial T}{\partial x}+v\frac{\partial T}{\partial y}=\alpha\frac{\partial^{2}T}{\partial y^{2}}+\tau\left[D_{B}\frac{\partial C}{\partial y}\frac{\partial T}{\partial y}+\left(\frac{D_{T}}{T_{\infty}}\right)\left(\frac{\partial T}{\partial y}\right)^{2}\right], \tag{3}$$

$$u\frac{\partial C}{\partial x}+v\frac{\partial C}{\partial y}=D_{B}\frac{\partial^{2}C}{\partial y^{2}}+\left(\frac{D_{T}}{T_{\infty}}\right)\frac{\partial^{2}T}{\partial y^{2}}, \tag{4}$$

where x and y denote the vertical and horizontal directions, respectively. u, v, T and C are the x- and y components of velocity, temperature and nanoparticles volume fraction, respectively. K, β, g, D_B and D_T are the permeability of the porous medium, volumetric expansion coefficient of fluid, gravitational acceleration, Brownian diffusion coefficient and the thermophoretic diffusion coefficient, respectively. K^*, γ, μ, ρ_f and ρ_p are the porous medium inertial coefficient, half angle of the cone, fluid dynamic viscosity, fluid density and nanoparticles mass density, respectively. $\alpha = k_m/(\rho c)_f$ and $\tau = (\rho c)_p/(\rho c)_f$ are the effective thermal diffusivity of the porous medium and the ratio of heat capacities, respectively. k_m, $(\rho c)_f$ and $(\rho c)_p$ are the effective thermal conductivity, heat capacity of the fluid and the effective heat capacity of the nanoparticles material, respectively.

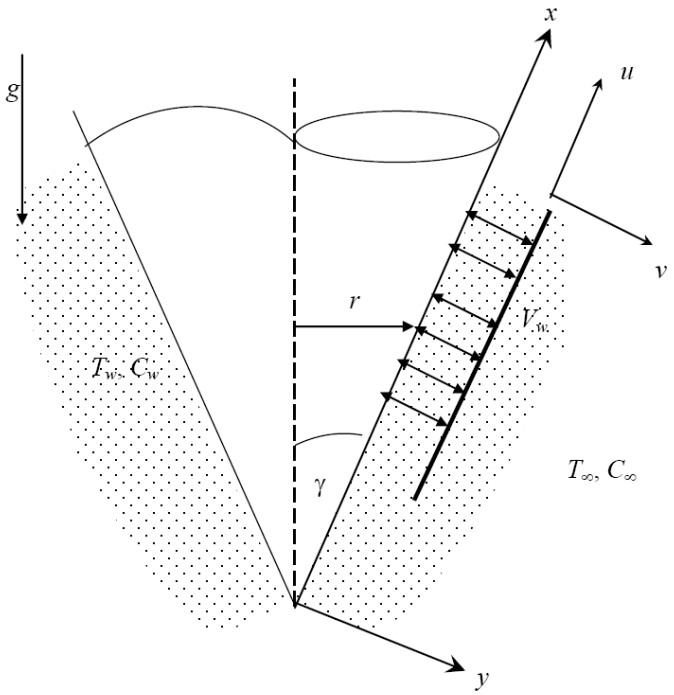

Figure 1. Flow model and physical coordinate system.

The boundary conditions suggested by the physics of the problem are given by

$$y = 0 : v = V_w \, , \; T = T_w \, , \; C = C_w \, , \tag{5a}$$

$$y \to \infty : u = 0, T = T_\infty, C = C_\infty, \tag{5b}$$

where V_w, T_∞ and C_∞ are the uniform transpiration velocity, temperature and nanoparticles volume fraction, respectively. It is assumed that the boundary layer is sufficiently thin in comparison with the local radius of the cone. Therefore, the local radius to a point in the boundary layer can be replaced by the radius of the cone r, i.e., $r = x \sin\gamma$. Introducing the stream function such that: $ru = \partial\psi / \partial y$, $rv = -\partial\psi / \partial x$ and substituting

$$\xi = \frac{2V_w x}{\alpha Ra_x^{1/2}}, \eta = \frac{y}{x} Ra_x^{1/2} \, , \; f(\xi,\eta) = \frac{\psi}{\alpha r Ra_x^{1/2}} \, , \; \theta(\xi,\eta) = \frac{(T - T_\infty)}{(T_w - T_\infty)} \, ,$$
$$\phi(\xi,\eta) = \frac{(C - C_\infty)}{(C_w - C_\infty)} \, , \tag{6}$$

into Eqs. (1) through (5) produces the following non-similar equations and boundary conditions:

$$f'' + 2Erf' f'' = \theta' - N_r \phi' \, , \tag{7}$$

$$\theta'' + N_b \phi' \theta' + \frac{3}{2} f \theta' + N_t \theta'^2 = \frac{1}{2} \xi \left(f' \frac{\partial\theta}{\partial\xi} - \theta' \frac{\partial f}{\partial\xi} \right), \tag{8}$$

$$\phi'' + \frac{3Le}{2} f \phi' + \frac{N_t}{N_b} \theta'' = \frac{Le}{2} \xi \left(f' \frac{\partial\phi}{\partial\xi} - \phi' \frac{\partial f}{\partial\xi} \right), \tag{9}$$

$$\eta = 0 : f = -\frac{\xi}{4}, \theta = 1, \phi = 1, \tag{10a}$$

$$\eta \to \infty : \theta = 0, \phi = 0 \, , \tag{10b}$$

where

$$Nr = \frac{(\rho_p - \rho_{f\infty})(C_w - C_\infty)}{\rho_{f\infty} \beta (T_w - T_\infty)(1 - C_\infty)} \, , \quad Nb = \frac{(\rho c)_p D_B (C_w - C_\infty)}{(\rho c)_f \alpha} \, ,$$
$$Nt = \frac{(\rho c)_p D_T (T_w - T_\infty)}{(\rho c)_f \alpha T_\infty} \, ,$$
$$Er = \left(\rho_{f\infty} K^* \alpha / d\mu \right) Ra_d \quad Le = \alpha / D_B \, ,$$
$$Ra_x = \left\{ (1 - C_\infty) \rho_{f\infty} g \cos\gamma \beta K (T_w - T_\infty) x / \alpha\mu \right\} \tag{11}$$

are the buoyancy ratio, Brownian motion parameter, thermophoresis parameter, Ergun number (non-Darcy number) based on the pore diameter *d*, Lewis number and the modified local Rayleigh number for the flow through the porous medium, respectively. It should be noted that the transpiration parameter $\xi = 0$ ($V_w = 0$) corresponds to an impermeable cone surface while $\xi > 0$ ($V_w > 0$) corresponds to the case of fluid injection and $\xi < 0$ ($V_w < 0$) corresponds to the case of fluid suction. It is important to note that the most nanofluids examined to date have large values for the Lewis number Le > 1 (see Nield and Kuznetsov [20]). For water nanofluids at room temperature with nanoparticles of 1-100 nm diameters, the Brownian diffusion coefficient D_B ranges from 4×10^{-4} to 4×10^{-12} m^{-2}/s. Furthermore, the ratio of the Brownian diffusivity coefficient to the thermophoresis coefficient for particles with diameters of 1-100 nm can be varied in the ranges of 2-0.02 for alumina, and from 2 to 20 for copper nanoparticles (see Buongiorno [21] for details). Hence, the variation of the non-dimensional parameters of nanofluids in the present study is considered to vary in the mentioned range.

Of special significance for this problem are the local Nusselt and Sherwood numbers. These physical quantities can be defined as:

$$Nu_x Ra_x^{-1/2} = -\theta'(\xi, 0)\,, \tag{12}$$

$$Sh_x Ra_x^{-1/2} = -\phi'(\xi, 0)\,. \tag{13}$$

3. NUMERICAL METHOD AND VALIDATION

The non-similar equations (7) through (9) are nonlinear and possess no analytical solution and must be solved numerically. The efficient, iterative, tri-diagonal, implicit finite-difference method discussed by Blottner [22] has proven to be adequate for the solution of such equations. The equations are linearized and then descritized using three points central difference quotients with variable step sizes in the η direction and using two-point backward difference formulae in the ξ direction with a constant step size. The resulting equations form a tri-diagonal system of algebraic equations that can be solved by the well-known Thomas algorithm (see Blottner [22]). The solution process starts at $\xi=0$ where Eqs. (10) through (12) are solved and then marches forward using the solution at the previous line of constant ξ until it reaches the desired value of ξ. Due to the nonlinearities of the equations, an iterative solution with successive over or under relaxation techniques is required. The convergence criterion required that the maximum absolute error between two successive iterations be 10^{-6}. The computational domain was made of 196 grids in the η direction and 101 grids in the ξ direction. A starting step size of 0.001 in the η direction with an increase of 1.035 times the previous step size and a constant step size in the ξ direction of 0.01 were found to give very accurate results. The maximum value of η (η_∞) which represented the ambient conditions was assumed to be 35. The step sizes employed were arrived at after performing numerical experimentations to assess grid independence and ensure accuracy of the results. The accuracy of the aforementioned numerical method was validated by direct comparisons with the numerical results reported earlier by Yih [19] at various values of ξ in the absence of the

inertial effect, nanoparticles volume fraction, Brownian motion and thermophoresis effects ($Er=N_r= N_b=N_t=0$). This comparison is presented in Table 1. It can be seen from this table that excellent agreement between the results exists. This favorable comparison lends confidence in the numerical results to be reported in the next section.

Table 1. Values of $-\theta'(\xi,0)$ for various values of ξ in the absence of nanoparticles volume fraction, Brownian motion and thermophoresis effects ($N_r= N_b=N_t=0$)

ξ	Yih [19]	Present results
0	0.7686	0.7686
2	0.3537	0.3537
4	0.1342	0.1342
6	0.0400	0.0400

4. RESULTS AND DISCUSSION

In this section, representative numerical results are displayed with the help of graphical illustrations. Computations were carried out for various values of the physical parameters such as the Ergun number (non-Darcy number) Er, buoyancy ratio parameter Nr , Brownian motion parameter *Nb*, thermophoresis parameter *Nt*, and the Lewis number Le .

Figures 2-4 present the effects of the Ergun number (non-Darcy number) Er on the longitudinal velocity, temperature, and the nanoparticles volume fraction profiles, as well as the axial distributions of the Nusslet number and the Sherwood number, respectively. It is observed that, as the Ergun number Er increases, both of the temperature and the nanoparticles volume fraction profiles increase, while the velocity profiles within the boundary layer decrease. This causes the value of the wall velocity gradient to increase whereas the negative values of the wall temperature and nanoparticles volume fraction slopes decrease yielding corresponding decreases in all of the local Nusselt and Sherwood numbers as evident from Figures 3 and 4. In addition, it is predicted that both the local Nusselt and Sherwood numbers decrease with increasing values of the transpiration parameter ξ.

Figures 5-7 show the effects of the buoyancy ratio parameter Nr on the longitudinal velocity, temperature, and the nanoparticles volume fraction profiles as well as the axial distributions of the Nusslet number and the Sherwood number, respectively. It is noted that the buoyancy ratio parameter Nr has a similar tendency as the Ergun number Er parameter such that as the buoyancy ratio parameter Nr increases, both of the temperature and the nanoparticles volume fraction profiles increase, while the velocity profiles within the boundary layer decreases.

This causes the value of the slope of the velocity profile at the wall to increase and the negative values of the wall slopes of the temperature and nanoparticles volume fraction profiles to decrease yielding corresponding decreases in all of the Nusselt and Sherwood numbers as clearly shown in Figures 6 and 7.

Figures 8-10 depict the effects of the Brownian motion parameter *Nb* on the velocity, temperature and nanoparticles volume fraction profiles as well as the axial distributions of the Nusslet number and the Sherwood number, respectively. It is observed that as the Brownian

motion parameter *Nb* increases, the velocity and temperature profiles increase while the nanoparticles volume fraction profiles decrease within the boundary layer. In addition, as the Brownian motion parameter *Nb* increases, the value of the Nusslet number decreases while the value of the Sherwood number increases.

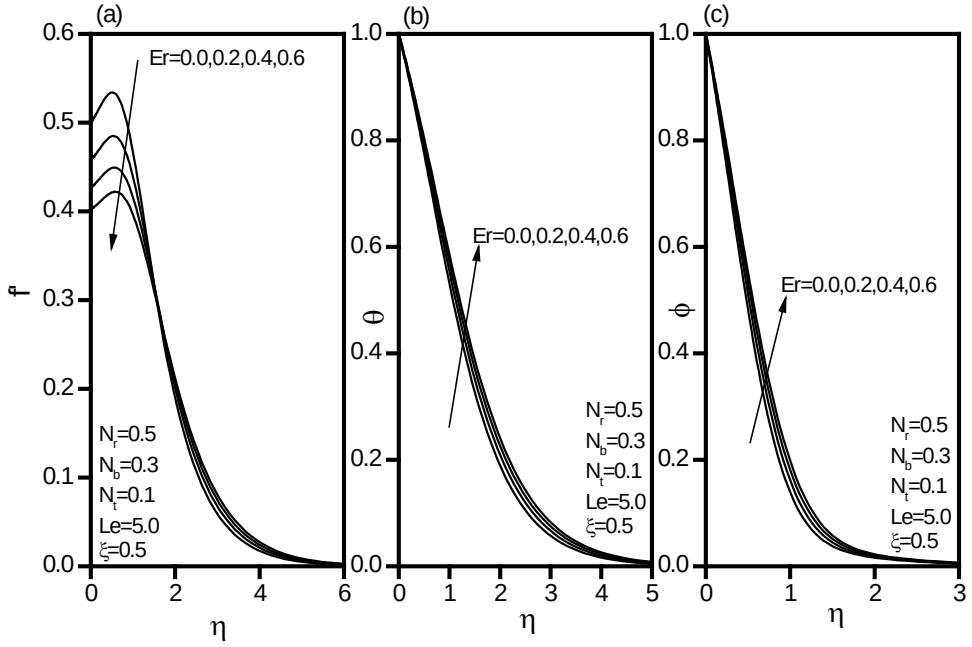

Figure 2. Effect of Er on the (a) velocity, (b) temperature, (c) volume fraction profiles.

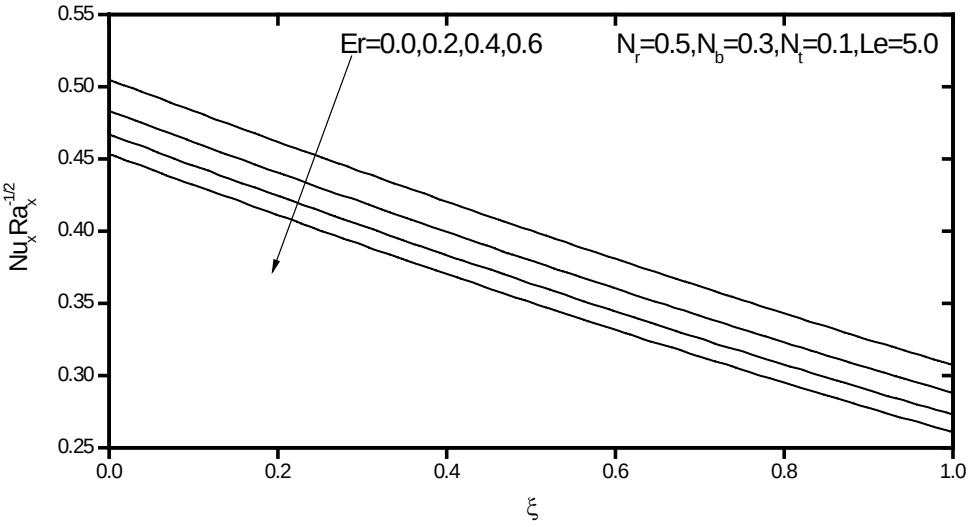

Figure 3. Effect of Er on the local Nusselt number.

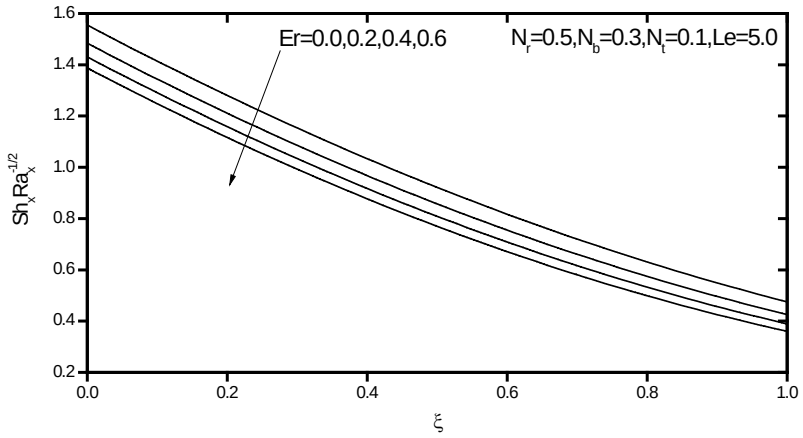

Figure 4. Effect of Er on the local Sherwood number.

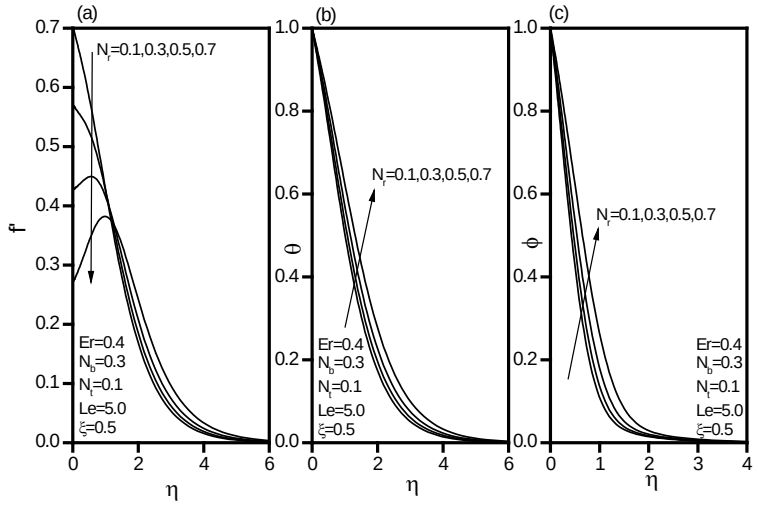

Figure 5. Effect of Nr on the (a) velocity, (b) temperature, (c) volume fraction profiles.

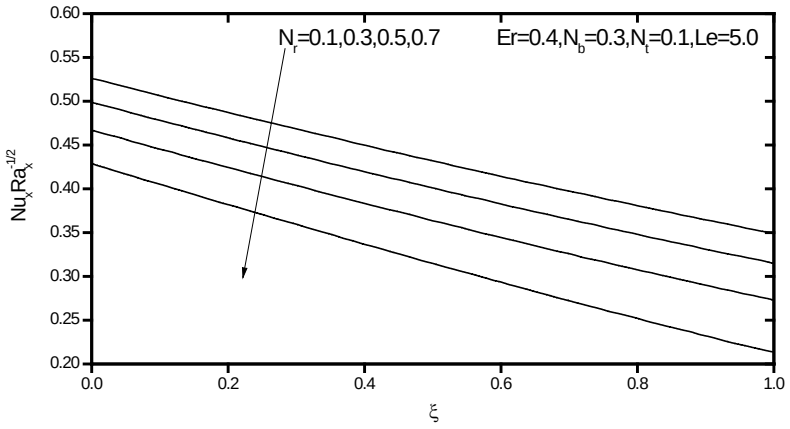

Figure 6. Effect of Nr on the local Nusselt number.

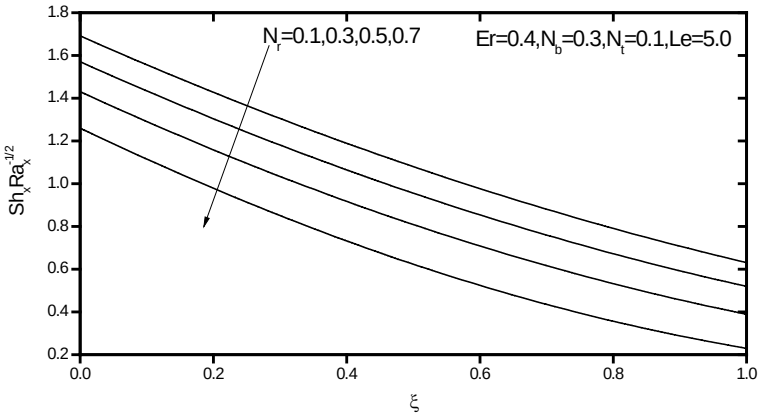

Figure 7. Effect of Nr on the local Sherwood number.

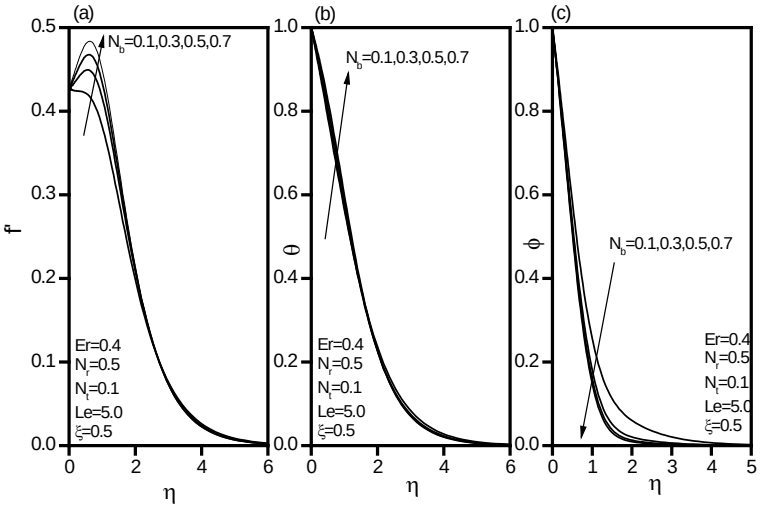

Figure 8. Effect of Nb on the (a) velocity, (b) temperature, (c) volume fraction profiles.

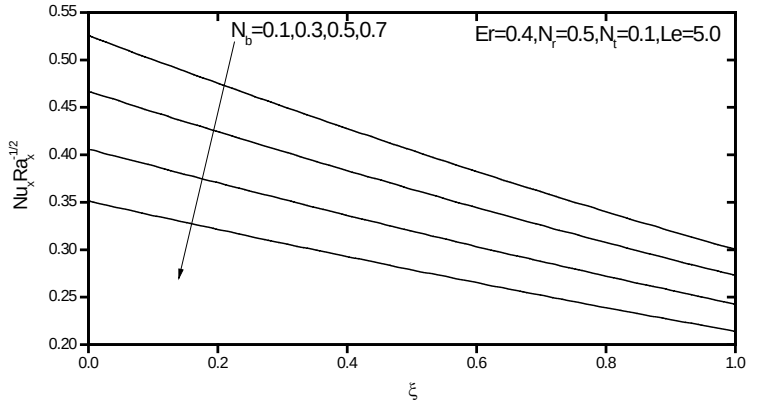

Figure 9. Effect of Nb on the local Nusselt number.

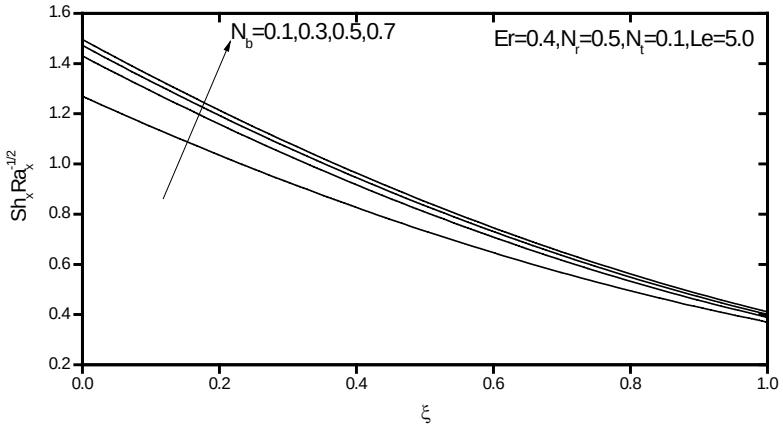

Figure 10. Effect of Nb on the local Sherwood number.

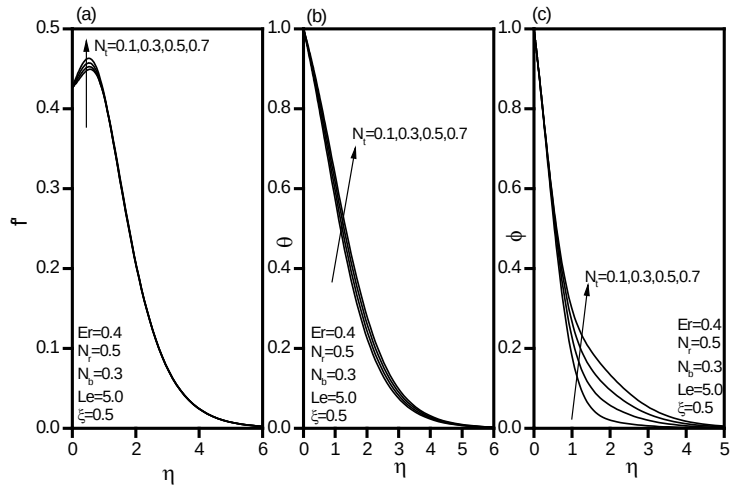

Figure 11. Effect of Nt on the (a) velocity, (b) temperature, (c) volume fraction profiles.

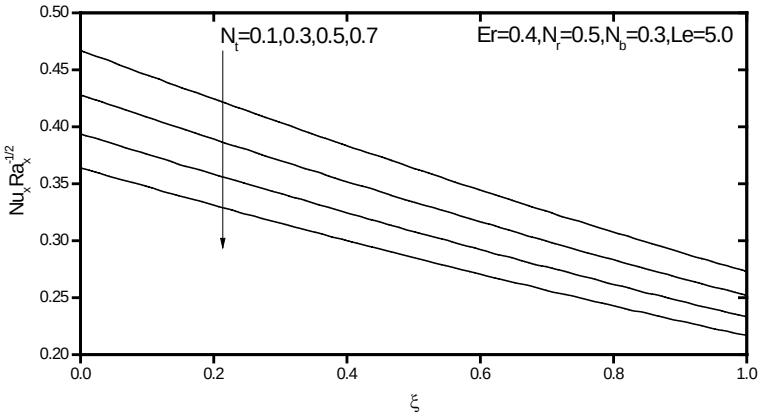

Figure 12. Effect of Nt on the local Nusselt number.

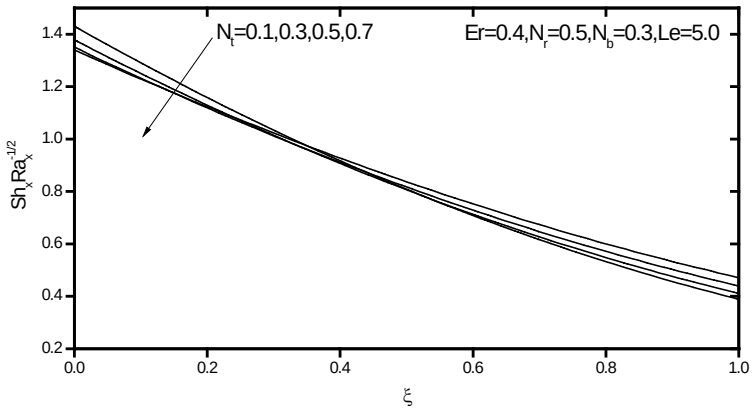

Figure 13. Effect of N_t on the local Sherwood number.

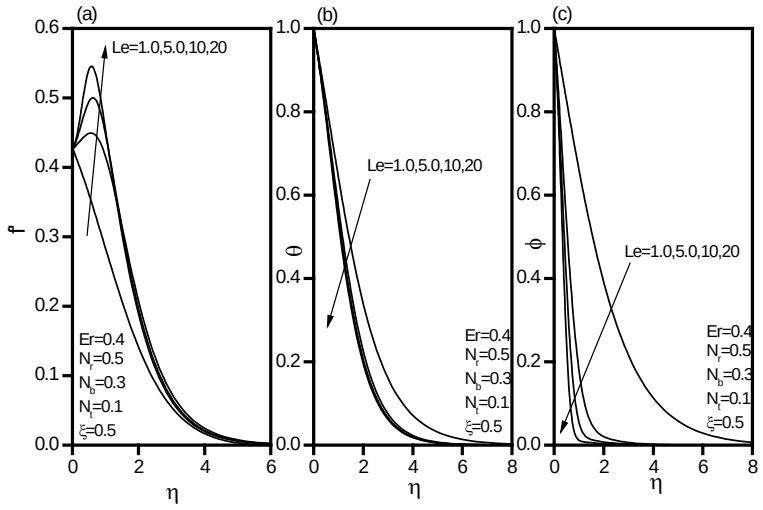

Figure 14. Effect of Le on the (a) velocity, (b) temperature, (c) volume fraction profiles.

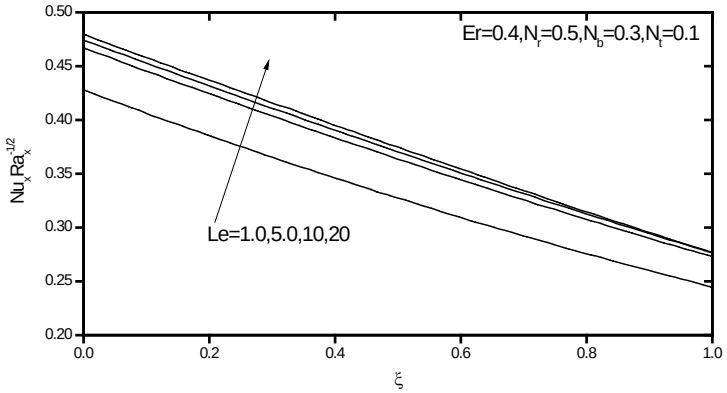

Figure 15. Effect of Le on the local Nusselt number.

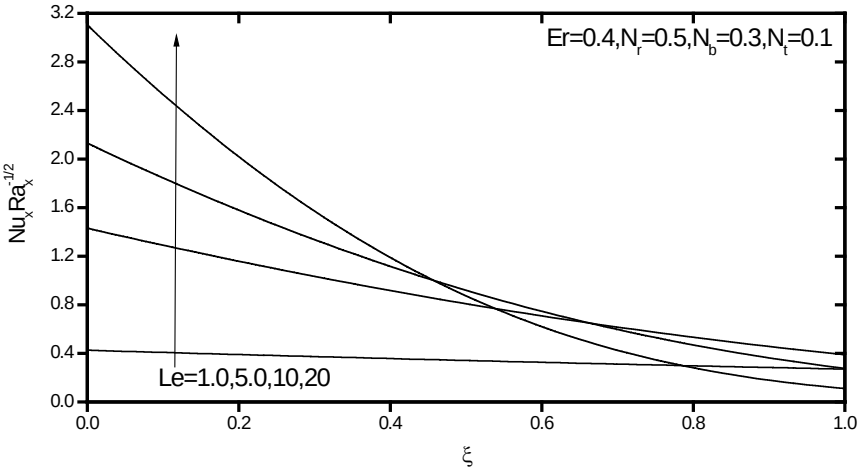

Figure 16. Effect of Le on the local Sherwood number.

This is due to the corresponding decrease in the negative value of the wall slope of the temperature profile and the increase in the negative value of the wall slope of the nanoparticles volume fraction profile, respectively.

Figures 11-13 elucidate the effects of the thermophoresis parameter *Nt* on the velocity, temperature and nanoparticles volume fraction profiles as well as the axial distributions of Nusslet number and the Sherwood number, respectively. It is clearly seen that as the thermophoresis parameter *Nt* increases, all of the velocity, temperature and nanoparticles volume fraction profiles increase.

In addition, it is predicted that the local Sherwood number decrease as the thermophoresis parameter *Nt* increases. Moreover, the local Nusslet number decreases as Nt increases for transpiration parameters $\xi < 0.35$, whereas the opposite behavior occurs for transpiration parameters $\xi > 0.35$.

Finally, Figures 14-16 illustrate the effects of the Lewis number on the velocity, temperature and the nanoparticles volume fraction profiles as well as the axial distributions of the Nusslet and Sherwood numbers, respectively. An increase in the value of the Lewis number *Le* is expected to cause sufficient decreases in the temperature and the nanoparticles volume fraction profile and their boundary layers and a weak increase in the velocity profile and its boundary layer. This leads to corresponding increases in the local Nusslet number. However, in general, as Le increases, the local Sherwood number increases for $\xi < 0.8$ whereas the opposite behavior occurs with increasing the transpiration parameter ξ>0.8 as evident from Figures 15 and 16.

CONCLUSION

An analysis was performed to study non-Darcy free convection boundary-layer flow over a permeable vertical cone embedded in a porous medium saturated with a nanofluid in the presence of uniform wall transpiration. The model used for the nanofluid incorporated the effects of Brownian motion and thermophoresis. Numerical results for the axial distributions

of the Nusselt and Sherwood numbers were presented for parametric variations of the buoyancy ratio parameter, Ergun number (non-Darcy number), Brownian motion parameter, thermophoresis parameter and the Lewis number. The results indicated that as either of the Ergun number (non-Darcy number) or the buoyancy ratio parameter increased, all of the Nusselt number and the Sherwood number decreased. Also, as the Brownian motion parameter increased, the Sherwood number increased whereas the Nusselt number decreased. In addition, as the thermophoresis parameter increased, the Nusselt and Sherwood numbers decreased. Furthermore, as the Lewis number increased, the Nusselt and Sherwood numbers increased. It was also predicted that the Nusselt and Sherwood numbers decreased with increasing values of the transpiration parameter.

ACKNOWLEDGMENTS

The authors are very thankful to the editor and the reviewers for their constructive comments and suggestions to improve the presentation of this paper.

REFERENCES

[1] K. Vafai, C.L. Tien, Boundary and inertia effects on flow and heat transfer in porous media, *Int. J. Heat Mass Transfer* 24 (1981) 195-203.

[2] P. Nithiarasu, K.N. Seetharamu, T. Sundararajan, Natural convective, heat transfer in a fluid saturated variable porosity medium, *Int. J. Heat Mass Transfer* 40 (1997) 3955-3967.

[3] R. F. Benenati, C.B. Brosilow, Void fraction distribution in packed beds, *AIChE J.* 8 (1962) 359-361.

[4] K. Vafai, Convective flow and heat transfer in variable porosity media, *J. Fluid Mechanics* 147 (1984) 233-259.

[5] K. Vafai, R.L. Alkire, C.L. Tien, An experimental investigation of heat transfer in variable porosity media, *ASME J. Heat Transfer* 107 (1985) 642-647.

[6] D. Poulikakos, K. Renken, Forced convection in a channel filled with Porous medium, including the effects of flow inertia, variable porosity, and Brinkman friction, *ASME J. Heat Transfer* 109 (1987) 880-888.

[7] P. Cheng, D. Vortmeyer, Transverse thermal dispersion and wall channeling in a packed bed with forced convective flow, *Chem. Eng. Sci.* 43 (1988) 2523-2532.

[8] Amiri, K. Vafai, Analysis of dispersion effects and non-thermal equilibrium, non-Darcian, variable porosity incompressible flow through porous media, *Int. J. Heat Mass Transfer* 37 (1994) 936-954.

[9] Y. Xuan, K. Yu, Q. Li, Investigation on flow and heat transfer of nanofluids by the thermal Lattice Boltzmann model, *Progress in Computational Fluid Dynamics* 5 (2005) 13-19.

[10] P. Keblinski, S.R. Phillpot, S. U. S. Choi, J. A. Eastman, Mechanisms of heat flow in suspensions of nano-sized particles (nanofluids), *Int. J. Heat Mass Transfer* 45 (2002) 855-863.

[11] S. K. Das, N. Putra, P. Thiesen, W. Roetzel, Temperature dependence of thermal conductivity enhancement for nanofluids, *J. Heat Transfer* 125 (2003) 567-574.
[12] N. Putra, W. Roetzel, S.K. Das, Natural convection of nano-fluids, *Heat Mass Transfer* 39 (2003) 775-784.
[13] D. Wen, Y. Ding, Natural convective heat transfer of suspensions of titanium dioxide nanoparticles (nanofluids), *IEEE Trans. Nanotechnol.* 5 (2006) 220-227.
[14] A. J. Chamkha, A.M. Aly, H. Al-Mudhaf, Laminar MHD mixed convection flow of a nanofluid along a stretching permeable surface in the presence of heat generation or absorption effects, *International Journal of Microscale and Nanoscale Thermal and Fluid Transport Phenomena* 2 (2011) 51-70.
[15] A. J. Chamkha, R.S.R. Gorla and K. Ghodeswar, Non-similar solution for natural convective boundary layer flow over a sphere embedded in a porous medium saturated with a nanofluid, *Transport in Porous Media* 86 (2010) 13-22.
[16] R. S. R. Gorla, S.M.M. EL-Kabeir, A.M. Rashad, Heat transfer in the boundary layer on a stretching circular cylinder in a nanofluid, *Journal of Thermophysics and Heat Transfer* 25 (2011) 183-186.
[17] R. S. R. Gorla, A. J. Chamkha, A.M. Rashad, Mixed convective boundary layer flow over a vertical wedge embedded in a porous medium saturated with a nanofluid, *Journal of Nanoscale Research Letters*, 2011, 6:207.
[18] S. Ergun, Fluid flow through packed columns, *Chem. Engng. Prog.* 48 (1952) 89-93.
[19] K. A. Yih, The effect of uniform lateral mass flux on free convection about a vertical cone embedded in a saturated porous medium, *Int. Comm. Heat Mass Transfer*, 24 (1997)1195-1205.
[20] D. A. Nield, A.V. Kuznetsov, Thermal instability in a porous medium layer saturated by a nanofluid, *Int. J. Heat and Mass Transfer*, 52(2009) 5796-5801.
[21] J. Buongiorno, Convective transport in nanofluids, *J. Heat Trans-T, ASME*, 128(2006) 241-250.
[22] F. G. Blottner, Finite-difference methods of solution of the boundary-layer equations, *AIAA Journal* 8 (1970) 193-205.

Received 21 February 2012, *received* in revised form 06 September 2012; *accepted* 13 September 2012.